Structure–Property Relationship of CaO-MgO-SiO_2 Slag: Quantitative Analysis of Raman Spectra

JOO HYUN PARK

The quantitative structural information such as the relative abundance of silicate discrete anions (Q^n units) and the concentration of three types of oxygens, *viz*. free-, bridging- and nonbridging oxygen can be obtained from micro-Raman spectra of the quenched CaO-SiO_2-MgO glass samples. Various transport properties such as viscosity, density, and electrical conductivity can be expected as a simple linear function of "ln (Q^3/Q^2)," indicating that these physical properties are strongly dependent on a degree of polymerization of silicate melts. The methodology outlined in the current study can be extended to predict the physicochemical properties of silicate melts in ferrous and non-ferrous metallurgical processes.

DOI: 10.1007/s11663-013-9825-9

I. INTRODUCTION

KNOWLEDGE of the structure of silicate melts is of great importance in metallurgical processes.[1,2] The structure of silicate melts is the dominant factor affecting the transport properties, such as viscosity, conductivity, density, *etc*. Therefore, there have been numerous attempts to measure and/or predict these macroscopic thermophysical properties as a function of the composition of silicates based on the microscopic view of structures.[3–21]

Viscosity (η) is of particular importance because it controls the rate of transport of matter and thus, of energy.[1,2,22] In general, the largest changes in the viscosity of silicate melts are found when metal oxides, MO (M = alkali, alkaline earth, *etc*.) are added to SiO_2. The associated variation of activation energy (E_η) follows similar trend. As the MO content increases, the structure transforms gradually to discrete polyanions, and finally to isolated SiO_4^{4-} ions.[18,19]

Over limited temperature intervals, electrical conductivity (κ) or resistivity (ρ_e) follows an Arrhenius law, as does viscosity. The activation energy for electrical conduction decreases slightly with increasing MO content. Bockris *et al*.[20] showed that electrical current is carried wholly by network-modifying cations, M^{n+}, indicating that silicate melts are only partially ionic and that anions must be large in size compared with cations. These authors also made the important observation that the activation energy is 2 to 5-fold smaller for electrical conduction than for viscous flow, indicating that these two properties are governed by different mechanisms with different energy barriers.[21]

Vibrational spectroscopy, specifically Raman spectroscopy was originally used to probe the local anionic structure of silicates.[22,23] The bands assigned to antisymmetric stretching of Si-O^- (non-bridging oxygen; NBO) and Si-O^0 (bridging oxygen; BO) bonds occur in the range from 850 to 1200 cm^{-1} region, whereas Si-O-Si bending modes are found between 500 and 700 cm^{-1}.[24] The frequencies of the stretching modes decrease with decreasing degree of polymerization, *viz*. increasing NBO/Si. There are several types of units such as SiO_2 (fully polymerized), Si_2O_5 (sheet), SiO_3 (chain), Si_2O_7 (dimmer), and SiO_4 (monomer).[22–32] Based on a nuclear magnetic resonance (NMR) spectra of silicates,[33–38] the stoichiometric notations for each unit were replaced by the so-called Q^n concept as follows: Q^4 (NBO/Si = 0), Q^3 (NBO/Si = 1), Q^2 (NBO/Si = 2), Q^1 (NBO/Si = 3), and Q^0 (NBO/Si = 4).

The structure of the CaO-SiO_2-MgO system, which is important in ferrous and non-ferrous metallurgical processes, was systematically investigated by McMillan using Raman spectroscopy.[39] The high-frequency Raman band (1050 cm^{-1}) increased and the 850 cm^{-1} band decreased in relative intensity as the silica content increased from 30 to 60 mol pct at CaO/MgO = 1. For the effect of the Ca↔Mg substitution on the distribution of silicate species at high silica region, *i.e*., SiO_2 = 70 mol pct, the relative proportion of Q^2/Q^3 groups increased as MgO substituted for CaO in the oxide structure. However, Chrissanthopoulos *et al*.,[40] based on analysis of the infrared spectra of sol–gel derived CaO-SiO_2-MgO glasses, reported that the concentrations of $Q^1 + Q^2$ or $Q^0 + Q^1$ species at 80 or 50 mol pct SiO_2, respectively, were enhanced in ternary system as compared with those in the CaO-SiO_2 and MgO-SiO_2 binary systems, in contrast to the results reported by McMillan.[39] Schneider *et al*.[41] analyzed ^{29}Si NMR measurements of the CaO-MgO-50 mol pct SiO_2 (CaO/MgO = 1) system and reported that the fraction of silicon species was as follows: $Q^0 + Q^1 = 0.16$ (±0.08), $Q^2 = 0.60$ (±0.1), and $Q^3 + Q^4 = 0.24$ (±0.07). However, the relative fractions of Q^n species for the CaO-MgO-SiO_2 (1:1:1 in mol ratio) system from Raman spectra were as follows: $Q^0 = 0.50$, $Q^1 = 0.35$,

JOO HYUN PARK, Professor, is with the Department of Materials Engineering, Hanyang University, Ansan 426-791, South Korea. Contact e-mail: basicity@hanyang.ac.kr
Manuscript submitted August 15, 2012.
Article published online May 11, 2013.

$Q^2 = 0.13$, and $Q^3 = 0.02$.[42] The discrepancies between these studies indicate that more structural information is needed for the CaO-SiO_2-MgO system, especially in the composition range of silica content is lower than 50 pct, which is highly important in metallurgical slags and fluxes.

Consequently, in the current study, the effects of CaO/SiO_2 ratio, SiO_2 content, and Ca↔Mg substitution on the distribution of silicate anionic species in the CaO-SiO_2-MgO slag system were investigated by micro-Raman spectroscopic analysis of melt-quenched glass samples. Furthermore, the relationships among the structural and physicochemical properties of silicate melts were evaluated.

II. EXPERIMENTAL PROCEDURE

A. *Preparation of Glass Samples*

Regent-grade SiO_2 powder (>99.9 pct purity) was used. CaO and MgO were obtained from reagent-grade $CaCO_3$ and $MgCO_3$ (>99.9 pct purity) calcined at 1273 K (1000 °C) for 10 hours. Powders of CaO, SiO_2, and MgO were weighed to obtain the required composition and mixed for 1 hour to obtain homogeneous mixtures. Mixtures were melted in a 20 cc platinum crucible at 1873 K (1600 °C) for 2 hours for homogenization and for bubble-free liquids under a purified Ar atmosphere. The Ar gas was highly purified by passing the gas through a silica gel and a furnace containing magnesium turnings at 723 K (450 °C), even though 99.999 pct purity gas was used.

After 2 hours, the crucible was quickly drawn from the furnace and the melt was rapidly quenched by pouring it into a copper mold in cooling water. Whole samples were confirmed to be in the glassy state by X-ray diffraction (Bruker D8 GADDS, Bruker AXS Inc., Madison, WI) using Cu Kα radiation (1.54 Å) with a generator power of 45 kV and 35 mA for 2θ from 10 to 90 deg. The compositions of glass samples were determined with an X-ray fluorescence spectroscope (Bruker S4 Explorer, Bruker AXS Inc., Madison, WI), as shown in Figure 1.

B. *Analysis of Raman Spectra*

Raman spectra of the glass samples were collected at room temperature in the range of 100 to 1900 cm^{-1} using an Ar excitation laser source with a wavelength of 514.5 nm coupled to Jobin–Yvon Horiba (LabRam HR, France) micro-Raman spectrometer. Raman shifts were measured with a precision of 0.3 cm^{-1} and the spectra resolution was of the order of 1 cm^{-1}. Quantitative peak deconvolution was carried out through the range of Raman shifts from 800 to 1200 cm^{-1}. The spectrum data were fitted by Gausssian function with an aid of the "PeakFit" program within ±0.5 pct error limit, and the relative abundance of Q^n units was calculated from the area fraction of the best-fitted Gaussian curves at the frequency for the symmetric stretching vibration of each Q^n unit.

Figure 2 shows a typical deconvolution result for the 40 mol pct CaO-20 mol pct MgO-40 mol pct SiO_2 system. Bands marked at 855, 905, 964, and 1056 cm^{-1} correspond to Q^0 (850 to 880 cm^{-1}), Q^1 (900 to 920 cm^{-1}), Q^2 (950 to 1000 cm^{-1}), and Q^3 (1050 to 1100 cm^{-1}) units, respectively.[22–33] The peak frequencies do vary some with composition within the above frequency ranges. Here, the Raman scattering for Q^4 unit (1200 and 1060 cm^{-1}) could not be resolved because of its very low intensity in mixed silicate systems, even though it was originally observed in vitreous silica glass.[22–33,39–43] This was recently confirmed by theoretical molecular dynamics (MD) calculations.[43]

Quantitative analysis of Raman spectra allowed determination of the configuration of each silicate unit from Q^0 to Q^3 according to bulk composition. The compositions and the relative area fractions of the fitted Gaussian bands are listed in Table I. Mysen *et al.*[22,28,29,31,32] concluded that the anionic structural units in the silicate melts are the same before and after quenching, and thus the structural features of quenched silicate glasses are applicable to molten silicates.

III. RESULTS AND DISCUSSION

A. *Effect of CaO/SiO_2 Ratio on the Structure of CaO-SiO_2-20 mol pct MgO System*

The Raman spectra of the CaO-SiO_2-20 mol pct MgO system (CaO/SiO_2 = 0.3 to 1.0) as a function of wavenumbers in the range from 700 to 1300 cm^{-1} are shown in Figure 3. It is easily found that the relative intensity of the high-frequency (1055 (±5) cm^{-1}) band significantly decreases with increasing CaO/SiO_2 ratio and becomes very week shoulder at CaO/SiO_2 = 1.0. Alternatively, the low-frequency (865 (±5) cm^{-1}) band increases in intensity with increasing CaO/SiO_2 ratio, and this tendency is profound at CaO/SiO_2 ratio greater than 0.6.

The relative fractions of the silicate anionic units obtained from Gaussian deconvolution of the Raman bands shown in Figure 3 are plotted against the CaO/SiO_2 ratio in Figure 4. The fraction of Q^3 unit continuously decreases, and the fractions of Q^2, Q^1, and Q^0 units increase with increasing CaO/SiO_2 ratio. This tendency qualitatively indicates that the silicate networks are depolymerized as the CaO/SiO_2 ratio increases at a fixed MgO content. It is noticeable that Q^3 and Q^2 units are most abundant, whereas Q^1 and Q^0 units are less than 10 pct, respectively. The silicates are mainly constituted by Q^2 (SiO_3-chain) unit (~64 pct), followed by Q^3 (Si_2O_5-sheet) unit (~18 pct), Q^0 (SiO_4-monomer) unit (~10 pct), and Q^1 (Si_2O_7-dimmer) unit (~8 pct) at CaO/SiO_2 = 1.0 composition.

In Figure 4, the Q^3/Q^2 ratio is also shown as a function of CaO/SiO_2 ratio. In the current study, the Q^3/Q^2 ratio is proposed as an index for the degree of polymerization of silicate networks based on the following equilibrium reaction among silicate units:[22,28,29,31,32]

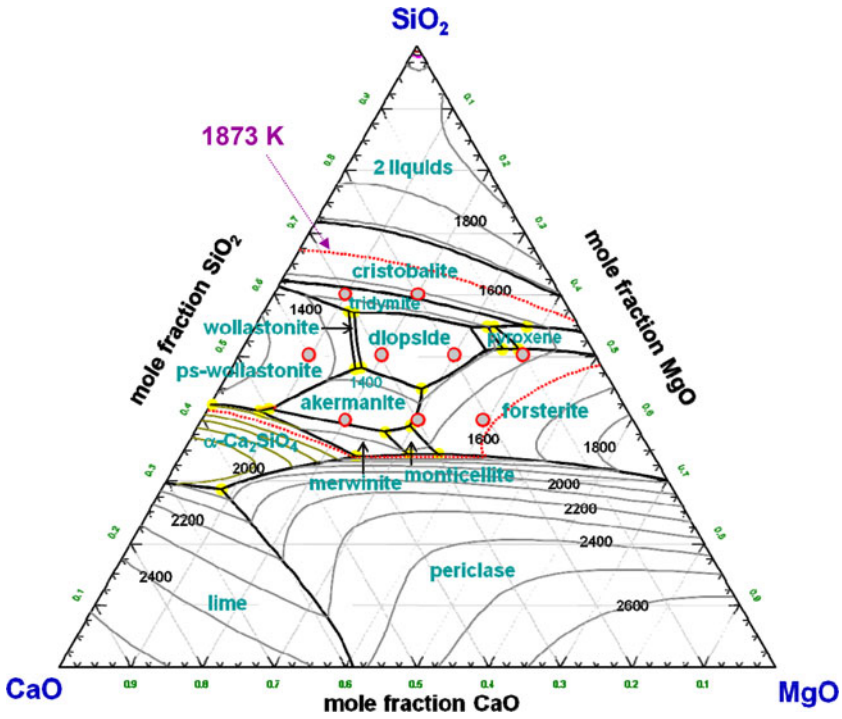

Fig. 1—Equilibrium phase diagram of the CaO-SiO_2-MgO slag and the composition of glass samples prepared in the current study.

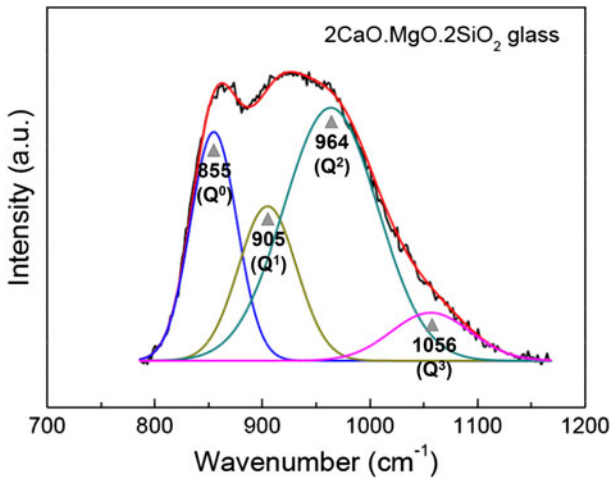

Fig. 2—Typical deconvolution of Raman spectra of 40 mol pct CaO-20 mol pct MgO-40 mol pct SiO_2 system.

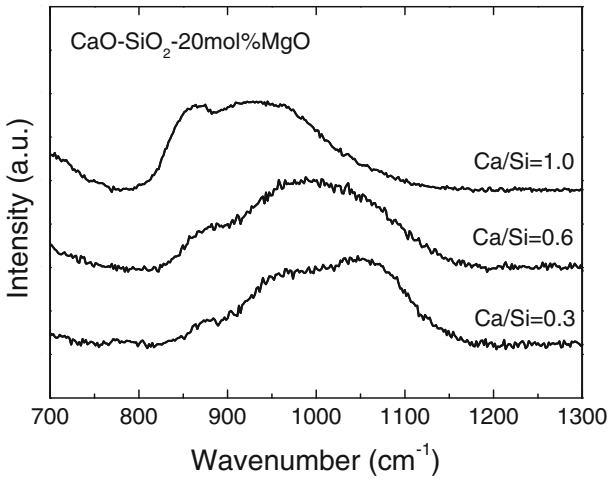

Fig. 3—Raman spectra of CaO-SiO_2-20 mol pct MgO system with CaO/SiO_2 ratio ranges from 0.3 to 1.0.

Table I. Composition of Glass Samples and the Peak Area Ratio obtained from a Gaussian Deconvolution of Raman Spectra

Composition, Mole Fraction			Best Fitted Gaussian Peak Area Ratio			
SiO_2	CaO	MgO	Q^3	Q^2	Q^1	Q^0
0.60	0.20	0.20	0.521	0.428	0.010	0.041
0.60	0.30	0.10	0.494	0.364	0.048	0.067
0.50	0.10	0.40	0.336	0.538	0.062	0.064
0.50	0.20	0.30	0.312	0.506	0.096	0.081
0.50	0.30	0.20	0.363	0.503	0.042	0.092
0.50	0.40	0.10	0.394	0.460	0.033	0.113
0.40	0.20	0.40	0.122	0.335	0.374	0.169
0.40	0.30	0.30	0.154	0.381	0.340	0.125
0.40	0.40	0.20	0.184	0.637	0.083	0.096

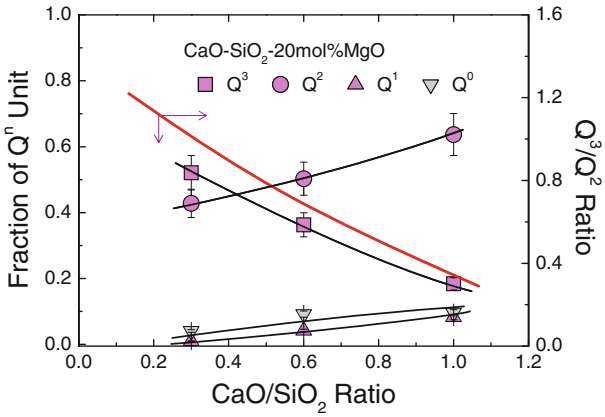

Fig. 4—Abundance of structural units and Q^3/Q^2 ratio in the CaO-SiO_2-20 mol pct MgO system as a function of CaO/SiO_2 ratio.

$$Si_2O_5 = SiO_3 + SiO_2 \quad [1]$$

$$K_{[1]} = \frac{[SiO_3]\cdot[SiO_2]}{[Si_2O_5]} = \frac{Q^2\cdot Q^4}{Q^3} \quad [2]$$

where $K_{[1]}$ is the equilibrium constant of Eq. [1]. Thus, the concentration of highly polymerized unit, *viz.* Q^4, is proportional to the concentration ratio of Q^3 to Q^2 (Eq. [3]) at a given temperature:

$$Q^4 = K_{[1]}\cdot\frac{Q^3}{Q^2} \propto \text{degree of polymerization} \quad [3]$$

The consideration of Eq. [3] is based on the fact that the Q^3 unit is the most polymerized unit which can be experimentally resolved by Raman spectroscopy as discussed in Section II–B.[22–43] The Q^3/Q^2 ratio continuously decreases from around 1.2 to 0.3 by increasing the CaO/SiO_2 ratio, and it becomes lower than unity at around $CaO/SiO_2 = 0.4$, which is consistent with the phase boundary of pure silica (tridymite) and Ca-Mg silicate (diopside; $CaMgSi_2O_6$) from the phase diagram of the CaO-SiO_2-MgO system as shown in Figure 1. From the viewpoint of structural similarity among silicate minerals, melts, and glasses,[22,28–32] the transition of the main silicate anionic unit from Q^3-sheet to Q^2-chain at the tridymite-diopside phase boundary in Figure 4 is theoretically reasonable because the structure of diopside is tetrahedral chain-like.[44–46]

B. *Effect of MgO Substitution for CaO on the Structure of CaO-SiO_2-MgO Slags*

The Raman spectra of the CaO-MgO-40 mol pct SiO_2 system ($MgO/(MgO + CaO) = 0.33$ to 0.67) as a function of wavenumbers in the range of 700 to 1300 cm^{-1} are shown in Figure 5. The relative intensity of the high-frequency (1055 ($\pm$5) cm^{-1}) band is very low, and it seems to be a weak shoulder in main silicate envelope. The intensity of this band decreases by the substitution of Mg^{2+} for Ca^{2+}. However, the changes in the intensity of the others are not easily discernible with human eyes.

The relative fractions of the silicate anionic units obtained from Gaussian deconvolution of the Raman bands shown in Figure 5 are plotted against the MgO/(MgO + CaO) ratio in Figure 6. The fraction of Q^2 unit sharply decreases, whereas that of Q^1 unit increases with increasing MgO/(MgO + CaO) ratio up to 0.5, followed by negligible changes. The changes in the fractions of Q^3 and Q^0 units are not significant. It is highly noticeable that the composition of MgO/(MgO + CaO) = 0.5 coincides exactly with the phase boundary between Ca-Mg silicate (akermanite; $Ca_2MgSi_2O_7$) and Mg silicate (forsterite; Mg_2SiO_4) from the CaO-MgO-SiO_2 phase diagram. Hence, the substitution of Mg^{2+} ion for Ca^{2+} ion in the Ca-Mg silicate affected the structure, whereas the Mg↔Ca substitution did not result in the significant change in the structure of Mg silicate, where the Ca^{2+} ions are relatively free compared with Mg^{2+} ions. This will be discussed more in detail later.

The Raman spectra of the CaO-MgO-50 mol pct SiO_2 system ($MgO/(CaO + MgO) = 0.2$ to 0.8) as a function of wavenumbers in the range of 700 to 1300 cm^{-1} are shown in Figure 7. The relative intensities of both the high (1055 ($\pm$5) cm^{-1})- and low (875 ($\pm$ 5) cm^{-1})-frequency bands decrease when Mg^{2+} substitutes for Ca^{2+} at a fixed silica content, *i.e.*, 50 mol pct. The relative fractions of the silicate anionic units obtained from Gaussian deconvolution of the Raman bands shown in Figure 7 are plotted against the MgO/(MgO + CaO) ratio in Figure 8. The fraction of Q^3 unit decreases and that of the Q^2 unit increases very slightly as the MgO/(MgO + CaO) ratio increases up to around 0.4, followed by negligible changes. The changes in the fractions of Q^3 and Q^0 units are not significant. The phase diagram of the CaO-MgO-SiO_2 system indicates that the substitution of Mg^{2+} for Ca^{2+} weakly modified the structure of Ca-silicate (pseudo-wollastonite; α-$CaSiO_3$) melt, while Mg↔Ca substitution did not result in significant changes in the diopside-like silicate structure.

The relationship between the Q^3/Q^2 ratio in the 40 and 50 mol pct SiO_2 systems and the MgO/(MgO + CaO) ratio is shown in Figure 9. In the 40 mol pct SiO_2 system, the Q^3/Q^2 ratio slightly increases as Mg^{2+} ion substitutes for Ca^{2+} ion in the akermanite primary area, whereas it is nearly constant irrespective of Mg↔Ca substitution in the forsterite primary area. From an analysis of McMillan,[39] doubly charged cations M^{2+} of large ionic radius, *i.e.*, small ionization potential ($=Z/r^2$) should preferentially occupy the more open, coupled Q^3 ($\equiv$Si-O^-)$_2$ sites, while smaller M^{2+} cations with larger ionization potential will favor the higher charge concentration offered by the Q^2 ($=$Si-$2O^-$) sites.

Because the ionization potential of Ca^{2+} ($Z/r^2 = 2.0$) is much lower than that of Mg^{2+} ($Z/r^2 = 3.9$),[47] the Ca^{2+} ion is charge balanced with two open O^- ions because of the large size of the [CaO_6] cage, whereas the Mg^{2+} ion is balanced with two adjacent corner-shared O^- ions because of the small size of the [MgO_6] cage. Hence, the increase in the MgO/(MgO + CaO) ratio increases the connectivity of silicate network in the

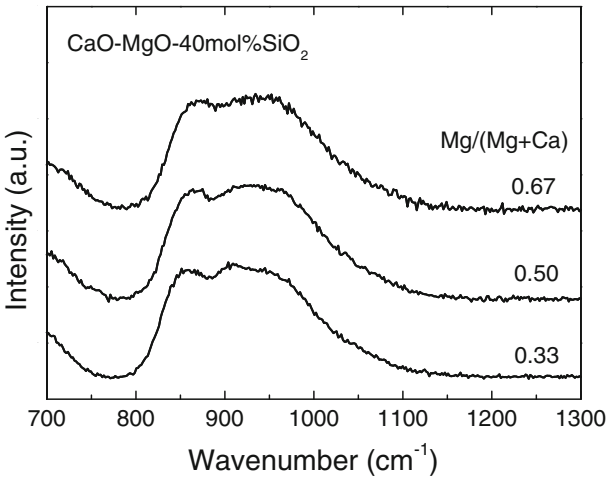

Fig. 5—Raman spectra of CaO–MgO–40 mol pct SiO_2 system with MgO/(MgO + CaO) ratios ranging from 0.33 to 0.67.

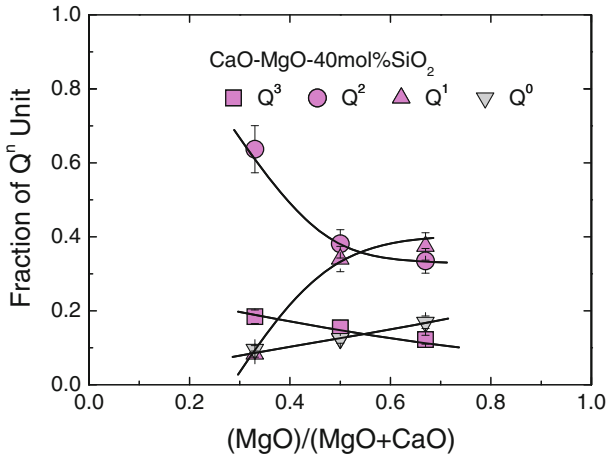

Fig. 6—Abundance of structural units in the CaO-MgO-40 mol pct SiO_2 system as a function of MgO/(MgO + CaO) ratio.

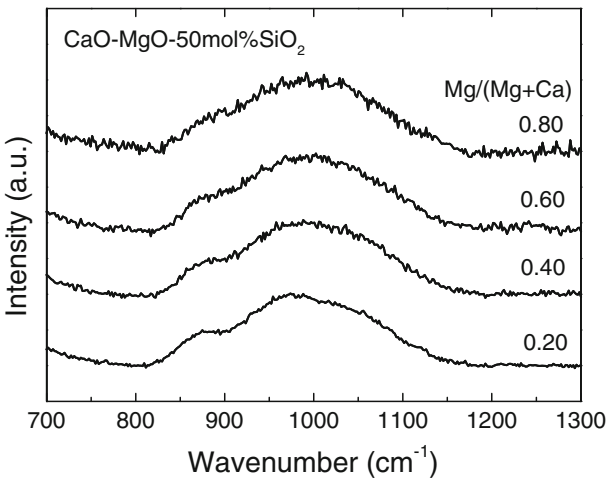

Fig. 7—Raman spectra of CaO-MgO-50 mol pct SiO_2 system with MgO/(MgO + CaO) ratio ranges from 0.2 to 0.8.

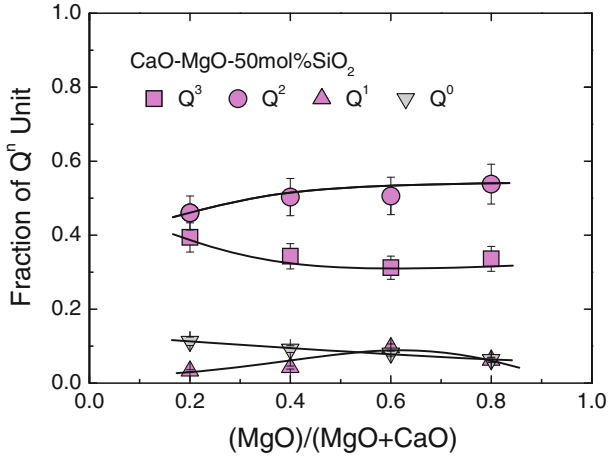

Fig. 8—Abundance of structural units in the CaO-MgO-50 mol pct SiO_2 system as a function of MgO/(MgO + CaO) ratio.

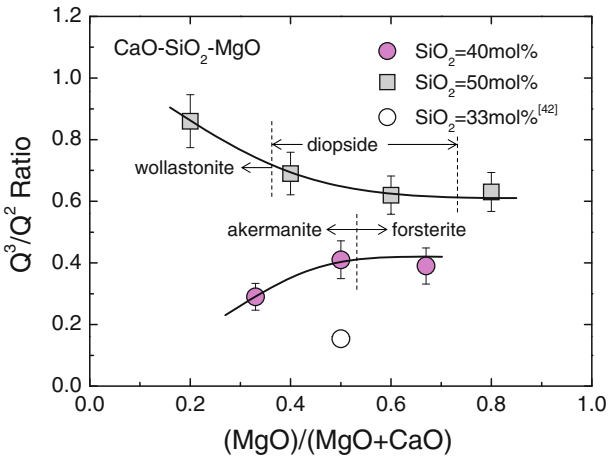

Fig. 9—The Q^3/Q^2 ratio of CaO-MgO-SiO_2 slags as a function of MgO/(MgO + CaO) ratio.

akermanite-like silicate structure, after which the forsterite-like silicate structure was not seriously affected by Mg↔Ca substitution because the abundant Mg^{2+} ions are strongly balanced with corner-shared O^- ions, while small amounts of Ca^{2+} ions are relatively free from a network-modifying role.

Alternatively, the value of Q^3/Q^2 ratio of the 50 mol pct SiO_2 system is higher than that of the 40 mol pct SiO_2 system, followed by that of 33 mol pct SiO_2 system at a fixed MgO/(MgO + CaO) ratio as shown in Figure 9. Also, the Q^3/Q^2 ratio slightly decreases as Mg^{2+} ion substitutes for Ca^{2+} ion in the (pseudo-) wollastonite primary area, whereas it is nearly constant irrespective of Mg↔Ca substitution in the diopside primary area. As discussed previously, the structure of silicate melts and glasses in the wollastonite primary area is similar to that of mineral phase,[22,28,29,31,32] which is known as layered ring-like structure at high temperatures.[48] Therefore, the relatively high connectivity of silicate network, balanced with abundant Ca^{2+} ions engaged in network-modifying role, decreases with increasing MgO/(MgO + CaO) ratio, followed by a less significant change in a diopside-like chain structure.

McMillan, based on an analysis of Raman spectra of the CaO-MgO-70 mol pct SiO_2 system, found that the 1060 cm^{-1} band (Q^3 unit) remained more intense than the shoulder at 980cm^{-1} (Q^2 unit) for MgO/(MgO + CaO) = 0.5 samples, but less so than for the 30 mol pct CaO-70 mol pct SiO_2 binary system.[39] The 30 mol pct MgO-70 mol pct SiO_2 system showed no resolved bands at high frequency, but only a broad asymmetric maximum between 960 and 1080 cm^{-1}, where the lower frequency part predominated. This observation indicated that the relative proportion of Q^3/Q^2 groups decreased as MgO substituted for CaO in the silicate structure.[39] McMillan's results for the 70 mol pct SiO_2 system are consistent with the present findings for the 50 mol pct SiO_2 system as shown in Figures 7 through 9.

C. *Structure–Property Relationship of the CaO-SiO_2-MgO Slags*

1. *Viscosity*

To understand the mechanism of viscous flow, it is necessary to relate the viscosity to the structure of silicates. Bridging oxygen bonds need to be broken and reformed for viscous flow. This observation is also consistent with the observation that the activation energy of viscous flow of silica-rich melts is comparable to the energy of Si-O bonds.[18,19,49] Consequently, it is possible that viscosity at a given temperature is a simple function of the abundance of fully polymerized structural units, such as Q^4. Clearly, viscosity (ln η) in simple binary alkali silicate melts is positively correlated with the concentration of Q^4 units.[49]

As discussed in Section III–A, because the Q^3/Q^2 ratio is directly proportional to the concentration of Q^4, the viscosity of the CaO-MgO-SiO_2 slag at 1873 K and 1773 K (1600 °C and 1500 °C) is plotted against the logarithm of the Q^3/Q^2 ratio in Figure 10. The viscosity of slag was calculated using FactSage™ 6.2 (ESM Software, Hamilton, OH) software to ensure consistent values through the wide temperature range. The details of the FactSage viscosity model are beyond the scope of the current study, but, the detailed information is provided in the literature (www.factsage.com).[50,51] The experimental data for the viscosity of specific compositions close to those of the glasses investigated in the current study are shown in Figure 10 for comparison.[52–55] The calculated and measured values are in good agreement. The viscosity of the silicate melts, ln η, increases linearly as ln (Q^3/Q^2) increases at 1873 K and 1773 K (1600 °C and 1500 °C).

The activation energy for the viscous flow of silicate melts in a Newtonian flow region above the liquidus temperature as a function of ln (Q^3/Q^2) is shown in Figure 11. The activation energy of silicate melts was obtained from an Arrhenius relationship (Eq. [4]) between viscosity and temperature:

$$\eta = \eta_o \exp\left(\frac{E_\eta}{RT}\right) \qquad [4]$$

As shown in Figure 11, the activation energy for the viscous flow of CaO-MgO-SiO_2 melts is a linear function of the degree of polymerization, which was defined as a function of ln (Q^3/Q^2) in the current study, as follows:

$$E_\eta(\text{kJ}) = 18.2(\pm 2.9) \cdot \ln\frac{Q^3}{Q^2} + 159.2(\pm 1.8) \quad (r^2 = 0.90) \qquad [5]$$

Consequently, the ln (Q^3/Q^2), which can be experimentally measured, can potentially be used as a good polymerization index to quantify the effect of silicate structure on the viscosity of the melts.

2. *Density*

Density (ρ) is one of the most useful variables for structural interpretation of molten oxides. Furthermore, the molar volume (V_m), which is the reciprocal of density ($V_m = M/\rho$, where M is the molar mass of molten silicates), is a thermodynamic property and directly reflects the Gibbs free energy of the oxide system.[1,22,56–62] It is also an important thermodynamic variable for calculating critical dimensionless numbers, *viz*. Reynolds, Prandtl, Nusselts, and Grashoffs numbers, which are used in heat and mass transfer calculations.[62]

The relationship between density of the CaO-MgO-SiO_2 melts at 1773 K (1500 °C) and ln (Q^3/Q^2) value is shown in Figure 12.[2,60] The density of melts linearly decreases as ln (Q^3/Q^2) increases at a given temperature with the following relationship:

$$\ln \rho(\text{g/cm}^3) = -0.0245(\pm 0.005) \cdot \ln\frac{Q^3}{Q^2} + 0.947(\pm 0.004) \; (r^2 = 0.88) \qquad [6]$$

Bottinga and Richet[59] discussed the effect of basic oxides, such as alkaline (*e.g.*, Na_2O) and alkaline earth oxides (*e.g.*, BaO), on the molar volume of binary silicates by gathering the experimental data measured by Bockris *et al.*[56,57] and Bruckner.[58] Based on the observation that the molar volume of pure liquid silica had a tendency to become smaller when network-modifying oxides were dissolved in pure SiO_2, despite their larger partial molar volume than that of SiO_2, Bottinga and Richet concluded that bridging oxygens have a larger partial molar volume than nonbridging oxygens.[22,59] The results shown in Eq. [6] and Figure 12 are consistent with their conclusion.

3. *Electrical conductivity*

Over limited temperature intervals, electrical conductivity (κ) follows an Arrhenius-type relationship, *viz*. Rasch–Hinrichsen law (Eq. [7]), similar to viscosity.[20–22]

$$\kappa = A \exp\left(\frac{E_\kappa}{RT}\right) \qquad [7]$$

The activation energy for electric conduction (E_κ) decreases slightly with an increase in the content of

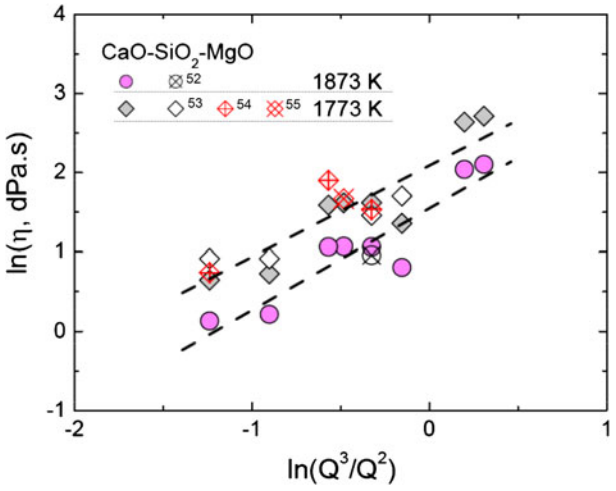

Fig. 10—Relationship between the viscosity and the Q^3/Q^2 ratio of $CaO-MgO-SiO_2$ melts at 1773 K and 1873 K (1500 °C and 1600 °C).

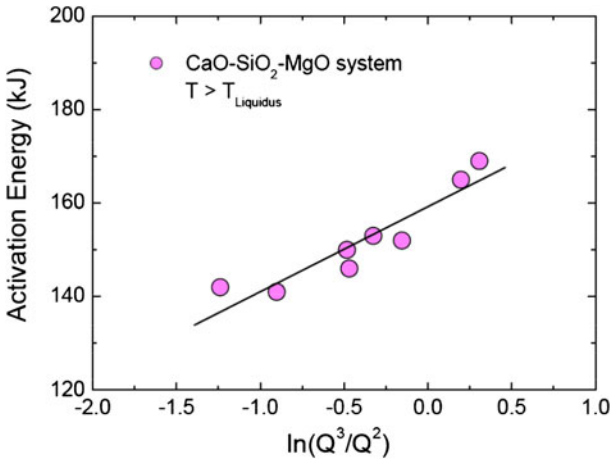

Fig. 11—Activation energy of viscous flow of $CaO–MgO–SiO_2$ melts as a function of Q^3/Q^2 ratio.

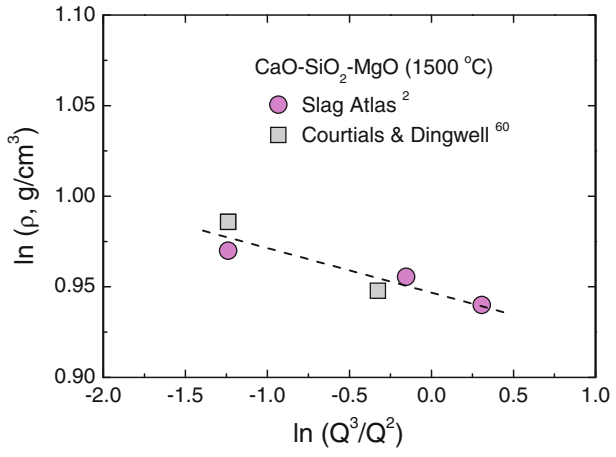

Fig. 12—Relationship between the density and the Q^3/Q^2 ratio of $CaO-MgO-SiO_2$ melts at 1773 K (1500 °C).

network-modifying oxides. Bockris *et al.*[20,21] showed that electrical current is carried wholly by network-modifying cations, M^{n+}, indicating that silicate melts are only partially ionic and that anions must be large in size compared with cations. Therefore, the electrical conductivity of molten silicates is strongly dependent on the degree of polymerization.

The relationship between the electrical conductivity (ln κ) and the degree of polymerization, *viz.* ln (Q^3/Q^2), of the $CaO-MgO-SiO_2$ melts at 1823 K (1550 °C) is shown in Figure 13;[2] ln κ decreases linearly as ln (Q^3/Q^2) increases with the following correlation that was obtained from a least square regression analysis.

$$\ln \kappa(\Omega^{-1}\,\mathrm{cm}^{-1}) = -0.82(\pm 0.11)\cdot \ln\frac{Q^3}{Q^2} - 1.16(\pm 0.07)\quad (r^2 = 0.90) \qquad [8]$$

Bockris *et al.*[20] concluded from their experimental results and absolute reaction rate theory that conductance due to O^{2-} ions is improbable, and the decrease in the activation energy with the increase in network-modifying oxides occurs because the breakdown of silicates facilitates cationic transport. The results shown in Figure 13 support Bockris *et al.*'s electrical conductance mechanism.[20–22]

D. *Speciation of Three Types of Oxygen from Raman Spectra*

The NBO/Si (measured) values of the $CaO-MgO-SiO_2$ silicates can be estimated from the following equation using a simple mass balance of oxygen and silicon atoms in each silicate unit, Q^n.

$$\mathrm{NBO/Si\ (meas.)} = \sum_{n=1}^{4} n \times (f_{Q^{4-n}}) \qquad [9]$$

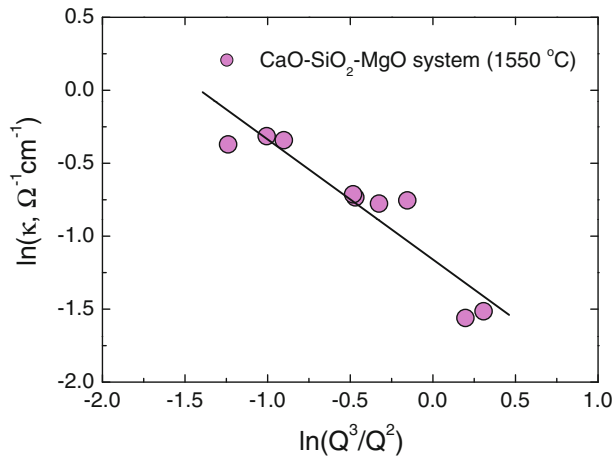

Fig. 13—Relationship between the electrical conductivity and the Q^3/Q^2 ratio of $CaO-MgO-SiO_2$ melts at 1823 K (1550 °C).

where $f_{Q^{4-n}}$ represents the area fraction of NBO/Si = n (Q^{4-n}) structure unit. Here, the theoretical NBO/Si (calculated) of silicates was obtained from Eq. [9].[2,16]

$$\text{NBO/Si (calc.)} = \frac{\sum 2X_{MO}}{X_{SiO_2}} \quad [10]$$

where X_{MO} is the mole fraction of oxide MO (M = Ca and Mg).

Figure 14 shows the relationship between the measured and the calculated values of NBO/Si of CaO-MgO-SiO_2 slags. We define here the *acidic region* in which the measured value is greater than the calculated one and vice versa for the *basic region*, respectively. The calculated NBO/Si is significantly overestimated at NBO/Si≅3, resulting from the fact that the silicate network is not perfectly depolymerized into the Q^0 (SiO_4) unit even in the highly basic composition. Thus some of the free oxygens (O^{2-}) locally interact with M^{2+} cations by the weak ionic bond rather than they are in global equilibrium with bridging and nonbridging oxygens by Eq. [11]. The network modifier free from the depolymerization reaction in the basic region is called the *excess base* in the current study.

$$O^0 + O^{2-} = 2O^- \quad [11]$$

$$K_{[11]} = \frac{(O^-)^2}{(O^0)\cdot(O^{2-})} \quad [12]$$

where $K_{[11]}$ is the equilibrium constant of Eq. [11].

On the other hand, in the acidic region, there are strong Si-O^0 bonds corresponding to the NBO/Si = 0 in the fully polymerized Q^4 silicate units even with very low concentrations, which could not be resolved within the analytic error limit in a deconvolution process because of very low intensity of the 1200 cm^{-1} bands in Raman spectra. Hence, the measured NBO/Si value which is greater than the calculated one in this acidic region (Figure 14) originates from the underestimation

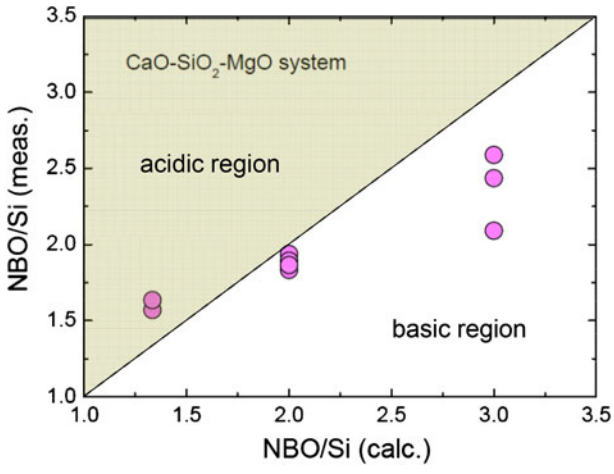

Fig. 14—Relationship between measured and calculated values of NBO/Si in the CaO-MgO-SiO_2 slags.

of the amount of bridging oxygen in the present analysis. The polymerized silica which was not experimentally resolved in the highly acidic region is called *excess silica* in the current study.

From the above findings, the mole fraction of O^{2-} and O^0 can be estimated from the measured amount of nonbridging oxygen, O^- as follows based on the mass balance of oxygen and silicon atoms. When NBO/Si(calc.)>NBO/Si(meas.), *i.e.*, in the relatively basic region,

$$X_{O^{2-}} = \frac{\text{excess base}}{2X_{SiO_2} + \sum X_{MO}}, \quad [13a]$$

$$\text{excess base} = \sum X_{MO} - \sum_{n=1}^{4} \frac{n}{2}\cdot\left(f_{Q^{4-n}}\right)\cdot X_{SiO_2} \quad [13b]$$

$$X_{O^-} = \left(1 - X_{O^{2-}}\right)\times\frac{\text{NBO/Si (meas.)}}{\text{NBO/Si (meas.)} + \sum_{n=1}^{4}\frac{(4-n)}{2}\times f_{Q^{4-n}}} \quad [14]$$

$$X_{O^0} = \left(1 - X_{O^{2-}}\right)\times\frac{\sum_{n=1}^{4}\frac{(4-n)}{2}\times f_{Q^{4-n}}}{\text{NBO/Si (meas.)} + \sum_{n=1}^{4}\frac{(4-n)}{2}\times f_{Q^{4-n}}} \quad [15]$$

The second term in the right-hand side of Eq. [13b] represents the amount of free oxygens consumed in a depolymerization reaction of silicate networks.

Alternatively, when NBO/Si(calc.)<NBO/Si(meas.), *i.e.*, in the relatively acidic region,

$$X_{O^o}^{excess} = \frac{2\times\text{excess silica}}{2X_{SiO_2} + \sum X_{MO}}, \quad [16a]$$

$$\text{excess silica} = X_{SiO_2} - \frac{\sum 2X_{MO}}{\text{NBO/Si (meas.)}} \quad [16b]$$

$$X_{O^-} = \left(1 - X_{O^o}^{excess}\right)\times\frac{\text{NBO/Si (meas.)}}{\text{NBO/Si (meas.)} + \sum_{n=1}^{4}\frac{(4-n)}{2}\times f_{Q^{4-n}}} \quad [17]$$

$$X_{O^0} = \left(1 - X_{O^o}^{excess}\right)\times\frac{\sum_{n=1}^{4}\frac{(4-n)}{2}\times f_{Q^{4-n}}}{\text{NBO/Si (meas.)} + \sum_{n=1}^{4}\frac{(4-n)}{2}\times f_{Q^{4-n}}} + X_{O^o}^{excess} \quad [18]$$

The relative concentrations of the three types of oxygen in the CaO-SiO_2-MgO slags are shown in Figure 15 as a function of mole fraction of silica. For comparison, the results for the binary silicate systems computed using cell model are also shown.[63] Figure 15

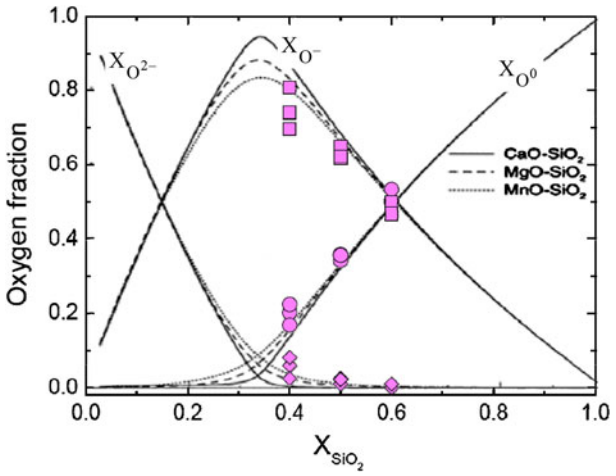

Fig. 15—Concentration of three types of oxygen in the CaO-MgO-SiO_2 slags as a function of mole fraction of silica.

shows that the orthosilicate composition ($X_{SiO_2} = 1/3$) can be considered as a breaking point.[63] At $X_{SiO_2} < 1/3$, the silicates consist of almost no BO, and the number of free oxygen decreases, while the number of NBO increases with increasing silica content. This is considered to have resulted from more oxygen ions becoming associated with silicon to form SiO_4^{4-} tetrahedra. At $X_{SiO_2} = 1/3$, the number of NBO reaches a maximum, which indicates that the majority of oxygen ions are configured in SiO_4^{4-} tetrahedra. When silica content exceeds this composition, free oxygen tends to disappear, and the number of NBO decreases, while the number of BO increases. This suggests that the SiO_4^{4-} tetrahedra are linked together to form large-sized silicate anions and develop into a network structure.[63]

In Figure 15, the concentration of bridging oxygen, X_{O^0} which increases with increasing mole fraction of silica in the composition range can be investigated at 1873 K (1600 °C), while the values X_{O^-} and $X_{O^{2-}}$ decrease as the content of silica increases. Because the content of free oxygen ions in silicate melts and glasses is significantly important in view of physicochemical properties, a number of scientists have developed several models based on the empirical and statistical approaches to quantify the content of free O^{2-} ions. Thus, the present methodology for the structural analysis of the silicate melts is very useful not only in view of the configuration of discrete anionic units at a given composition but also the concentration of free oxygen ions.

IV. CONCLUSIONS

The quantitative structural information such as the relative abundance of silicate discrete anions (Q^n units) and the concentration of three types of oxygens, *viz*. free oxygen, bridging oxygen, and nonbridging oxygen can be obtained from micro-Raman spectra of the quenched $CaO-SiO_2$-MgO glasses. Various thermophysical properties, such as viscosity, density (and molar volume), and electrical conductivity (and resistance) can be expected as a simple linear function of ln (Q^3/Q^2), indicating that these physical properties are strongly dependent on the degree of polymerization of silicate melts. Consequently, costly and time-consuming experiments for the measurements of several important properties of silicate melts can potentially be omitted. Just simple glassmaking and quantitative analysis of Raman bands are required instead. The present methodology can be extended to predict the physicochemical properties of silicate melts in ferrous and non-ferrous metallurgical processes.

ACKNOWLEDGMENT

The author would like to thank Prof. Em. K.C. MILLS, Imperial College London, UK, and Prof. Y. SASAKI, GIFT, POSTECH, Korea for their helpful discussions on this topic.

REFERENCES

1. Y. Waseda and J.M. Toguri: *The Structure and Properties of Oxide Melts,* World Scientific Publishing, Singapore, 1998.
2. K.C. Mills: *Slag Atlas*, 2nd ed. Verlag Stahleisen GmbH, Düsseldorf, Germany, 1995.
3. B. Cochain, D.R. Neuville, G.S. Henderson, C.A. McCammon, O. Pinet, and P. Richet: *J. Am. Ceram. Soc*., 2012, vol. 95, pp. 962–71.
4. H. Kim, W.H. Kim, J.H. Park, and D.J. Min: *Steel Res. Int*., 2010, vol. 81, pp. 17–24.
5. J.H. Park, H. Kim, and D.J. Min: *Metall. Mater. Trans. B*, 2008, vol. 39B, pp. 150–53.
6. J.H. Park and D.J. Min: *ISIJ Int*., 2007, vol. 47, pp. 1368–69.
7. X. Hou, R.J. Kirkpatrick, L.J. Struble, and P.J.M. Monteiro: *J. Am. Ceram. Soc*., 2005, vol. 88, pp. 943–49.
8. S. Seetharaman, K. Mukai and Du Sichen: *Steel Res. Int*., 2005, vol. 76, pp. 267–78.
9. R.E. Aune, M. Hayashi, and S. Sridhar: *Ironmak. Steelmak*., 2005, vol. 32, pp. 141–50.
10. J.H. Park and D.J. Min: *J. Non-Cryst. Solids*, 2004, vol. 337, pp. 150–56.
11. J.H. Park, D.J. Min, and H.S. Song: *Metall. Mater. Trans. B*, 2004, vol. 35B, pp. 269–75.
12. J.H. Park, D.J. Min, and H.S. Song: *Metall. Mater. Trans. B*, 2002, vol. 33B, pp. 723–29.
13. J.H. Park, D.J. Min, and H.S. Song: *ISIJ Int*., 2002, vol. 42, pp. 344–51.
14. J.H. Park and P.C.H. Rhee: *J. Non-Cryst. Solids*, 2001, vol. 282, pp. 7–14.
15. S. Sridhar, K.C. Mills, O.D.C. Afrange, H.P. Lorz, and R. Carli: *Ironmak. Steelmak*., 2000, vol. 27, pp. 238–42.
16. K.C. Mills: *ISIJ Int*., 1993, vol. 33, pp. 148–55.
17. G. Urbain and M. Boiret: *Ironmak. Steelmak*., 1990, vol. 17, pp. 255–60.
18. J.O'M. Bockris, J.D. Mackenzie and J.A. Kitchener: *Trans. Faraday Soc.,* 1955, vol. 51, pp. 1734–48.
19. J.O'M. Bockris and D.C. Lowe: *Proc. Roy. Soc. London A,* 1954, vol. 226A, pp. 423–35.
20. J.O'.M. Bockris, J.A. Kitchener, S. Ignatowicz, and J.W. Tomlinson: *Trans. Faraday Soc*., 1952, vol. 48, pp. 75–91.
21. J.O'.M. Bockris, J.A. Kitchener, and A.E. Davies: *Trans. Faraday Soc*., 1952, vol. 48, pp. 536–48.
22. B.O. Mysen and P. Richet: *Silicate Glasses and Melts: Properties and Structure*. Elsevier, Amsterdam, The Netherlands, 2005.
23. J. Etchepare: *Study by Raman Spectroscopy of Crystalline and Glassy Diopside*, in Amorphous Materials, eds. R. W. Douglas and E. Ellis, Wiley-Interscience, New York, NY, 1972.
24. T. Furukawa, K.E. Fox, and W.B. White: *J. Chem. Phys*., 1981, vol. 75, pp. 3226–37.

25. S.A. Brawer and W.B. White: *J. Non-Cryst. Solids*, 1977, vol. 23, pp. 261–78.
26. S.A. Brawer and W.B. White: *J. Chem. Phys.*, 1975, vol. 63, pp. 2421–32.
27. P. McMillan: *Am. Mineral.*, 1984, vol. 69, pp. 622–44.
28. D. Virgo, B.O. Mysen, and I. Kushiro: *Science*, 1980, vol. 208, pp. 1371–73.
29. B.O. Mysen: *Am. Mineral.*, 1980, vol. 65, pp. 690–710.
30. M.B. Silva, C.M. Queiroz, S. Agathopoulos, R.N. Correia, M.H.V. Fernandes, and J.M. Oliveira: *J. Mol. Struc.*, 2011, vol. 986, pp. 16–21.
31. B.O. Mysen: *Eur. J. Mineral.*, 2003, vol. 15, pp. 781–802.
32. B.O. Mysen: *Earth Sci. Rev.*, 1990, vol. 27, pp. 281–365.
33. M. Schramm, B.H.W.S. DeJong, and V.F. Parziale: *J. Am. Chem. Soc.*, 1984, vol. 106, pp. 4396–4402.
34. J.F. Stebbins, J.B. Murdoch, E. Schneider, I.S.E. Carmichael, and A. Pines: *Nature*, 1985, vol. 314, pp. 250–52.
35. J.F. Stebbins: *Nature*, 1987, vol. 330, pp. 465–67.
36. J.F. Stebbins and I. Farnan: *Science*, 1989, vol. 245, pp. 257–63.
37. J.F. Stebbins and I. Farnan: *Science*, 1992, vol. 255, pp. 586–89.
38. J.F. Stebbins and Z. Xu: *Nature*, 1997, vol. 390, pp. 60–62.
39. P. McMillan: *Am. Mineral.*, 1984, vol. 69, pp. 645–59.
40. A. Chrissanthopoulos, N. Bouropoulos, and S.N. Yannopoulos: *Vib. Spectrosc.*, 2008, vol. 48, pp. 118–25.
41. J. Schneider, V.R. Mastelaro, E.D. Zanotto, B.A. Shakhmatkin, N.M. Vedishcheva, A.C. Wright, and H. Panepucci: *J. Non-Cryst. Solids*, 2003, vol. 325, pp. 164–78.
42. N.K. Nasikas, A.A. Chrissanthopoulos, N. Bouropoulos, S. Sen, and G.N. Papatheodorou: *Chem. Mater.*, 2011, vol. 23, pp. 3692–97.
43. Y.Q. Wu, G.C. Jiang, J.L. You, H.Y. Hou, H. Chen, and K.D. Xu: *J. Chem. Phys.*, 2004, vol. 121, pp. 7883–95.
44. L.W. Finger and Y. Ohashi: *Am. Mineral.*, 1976, vol. 61, pp. 303–10.
45. L. Levien and C.T. Prewitt: *Am. Mineral.*, 1981, vol. 66, pp. 315–23.
46. R.M. Thompson and R.T. Downs: *Am. Mineral.*, 2008, vol. 93, pp. 177–86.
47. R.D. Shannon: *Acta Crystallogr. A*, 1976, vol. 32A, pp. 751–67.
48. H. Yang and C.T. Prewitt: *Am. Mineral.*, 1999, vol. 84, pp. 929–32.
49. B.O. Mysen: *Phys. Earth Planet. In.*, 1998, vol. 107, pp. 23–32.
50. A.N. Grundy, H. Liu, I.H. Jung, S.A. Decterov, and A.D. Pelton: *Int. J. Mater. Res.*, 2008, vol. 99, pp. 1185–94.
51. A.N. Grundy, I.H. Jung, A.D. Pelton, and S.A. Decterov: *Int. J. Mater. Res.*, 2008, vol. 99, pp. 1195–1209.
52. G. Urbain, Y. Bottinga, and P. Richet: *Geochim. Cosmochim. Acta*, 1982, vol. 46, pp. 1061–72.
53. Y. Kawai and Y. Shiraishi: *Handbook of Physico–chemical Properties at High Temperatures*, The Iron and Steel Institute of Japan, Tokyo, 1988.
54. T. Licko and V. Danek: *Phys. Chem. Glasses*, 1986, vol. 27, pp. 22–26.
55. A.M. Scarfe and D.J. Cronin: *Am. Mineral.*, 1986, vol. 71, pp. 767–71.
56. J.O'M. Bockris, J.W. Tomlinson and J.L. White: *Trans. Faraday Soc.,* 1956, vol. 53, pp. 299–310.
57. J.W. Tomlinson, M.S.R. Heynes and J.O'M. Bockris: *Trans. Faraday Soc.,* 1958, vol. 54, pp. 1822–33.
58. R. Bruckner: *Glastech. Ber.*, 1964, vol. 37, pp. 459–75.
59. Y. Bottinga and P. Richet: *Geochim. Cosmochim. Acta*, 1995, vol. 59, pp. 2725–31.
60. P. Courtial and D.B. Dingwell: *Am. Mineral.*, 1999, vol. 84, pp. 465–76.
61. Y. Linard, H. Nonnet, and T. Advocat: *J. Non-Cryst. Solids*, 2008, vol. 354, pp. 4917–26.
62. L. Muhmood and S. Seetharaman: *Metall. Mater. Trans. B*, 2010, vol. 41B, pp. 833–40.
63. L. Zhang and S. Jahanshahi: *Metall. Mater. Trans. B*, 1998, vol. 29B, pp. 177–86.